Food and Chemical Toxicology 197 (2025) 115246

Contents lists available at ScienceDirect

Food and Chemical Toxicology

journal homepage: www.elsevier.com/locate/foodchemtox

Exposure to airborne particulate matter and undernutrition in young rats: An in-depth histopathological and biochemical study on lung and excretory organs

Ivana Masci [a], Carola Bozal [b], Christian Lezón [c], Maximiliano Martin [d], Fernando Brites [d], Julián Bonetto [a], Laura Alvarez [e], Melisa Kurtz [a,*], Deborah Tasat [a,f]

[a] Laboratorio de Bio-Toxicología Ambiental, Instituto de Tecnologías Emergentes y Ciencias Aplicadas. Escuela de Ciencia y Tecnología, Universidad Nacional de San Martín – CONICET, San Martín, Buenos Aires, Argentina
[b] Cátedra de Histología y Embriología. Facultad de Odontología, Universidad de Buenos Aires, Buenos Aires, Argentina
[c] Cátedra de Fisiología. Facultad de Odontología, Universidad de Buenos Aires, Buenos Aires, Argentina
[d] Laboratorio de Lípidos y Lipoproteínas, Departamento de Bioquímica Clínica. Facultad de Farmacia y Bioquímica, Universidad de Buenos Aires, Buenos Aires, Argentina
[e] Laboratorio de Efectos Biológicos de Contaminantes Ambientales, Departamento de Bioquímica Humana. Facultad de Medicina, Universidad de Buenos Aires, Buenos Aires, Argentina
[f] Cátedra de Anatomía Patológica. Facultad de Odontología, Universidad de Buenos Aires, Buenos Aires, Argentina

ARTICLE INFO

Handling Editor: Dr. Bryan Delaney

Keywords:
Air pollution
Malnutrition
Excretory organs
Histopathology
Oxidative stress
Inflammation

ABSTRACT

Environmental stressors, such as air particulate matter (PM) and nutrient deficiencies, can significantly impact crucial organs involved in detoxifying xenobiotics, including lungs, liver, and kidneys, especially in vulnerable populations like children. This study investigated the effect of 4-week exposure to Residual Oil Fly Ash (ROFA) on these organs in young rats under growth-restricted nutrition (NGR). We assessed histological, histomorphometric and biochemical parameters. ROFA exposure induced histological changes and inflammation in all three organs when compared to control (C) animals. Specifically, in lungs ROFA caused a significant reduction in alveolar airspace (C: 55.8 ± 1.8% vs. ROFA: 38.7 ± 3.0%, $p < 0.01$) and alveolar number along with changes in alveolar size distribution, and disruption of the smooth muscle layer which may impaired respiratory function. In the liver, ROFA increased binucleated cells, macro and microvesicles and both AST and ALT serum biomarkers (AST: C = 77.7 ± 1.3 vs. ROFA = 81.6 ± 1.3, $p < 0.05$; ALT: C = 44.5 ± 0.9 vs. ROFA = 49.4 ± 1.3, $p < 0.05$). In the kidneys, a reduced Bowman's space (C: 2.15 ± 0.2 mm^2 vs. ROFA: 1.74 ± 0.2 mm^2, $p < 0.05$) was observed, indicative of glomerular filtration failure. NGR alone reduced Bowman's space (C: 2.15 ± 0.2 mm^2 vs. NGR: 1.06 ± 0.1 mm^2, $p < 0.001$). In lung and liver NGR showed higher levels of proinflammatory cytokine IL-6 ($p < 0.01$ and $p < 0.001$, respectively) when compared to C. In conclusion, both stressors negatively affected lung and excretory organs in young rats, with nutritional status further modulating the physiological response to ROFA. These findings highlight the compounded risks posed by environmental pollutants and poor nutrition in vulnerable populations.

1. Introduction

Air pollution and malnutrition are global challenges, posing significant public health risks. These two environmental stressors often coexist across different regions of the world, with South America, Africa, and Asia being the most affected continents, where large populations face the combined impact of both issues. Young children, especially those facing nutritional growth restrictions, are particularly vulnerable to the synergistic impacts of these stressors.

Exposure to air pollution, especially to particulate matter (PM), has been associated with a wide range of adverse health outcomes. PM is a complex mixture of solid and liquid particles suspended in the air, originated from various sources such as industrial processes, vehicle emissions, and the combustion of fossil fuels. Epidemiological and toxicological studies have demonstrated that PM contributes to respiratory diseases, including asthma, pneumonia, chronic obstructive

* Corresponding author.
E-mail address: mkurtz@unsam.edu.ar (M. Kurtz).

https://doi.org/10.1016/j.fct.2025.115246
Received 10 November 2024; Received in revised form 13 December 2024; Accepted 7 January 2025
Available online 9 January 2025

pulmonary disease (COPD), and lung cancer, as well as increased cardiovascular morbidity and mortality (Mills et al., 2009; Mills et al., 2011; Wellenius et al., 2012). PM exposure is known to elicit both short- and long-term effects on human health, including reduced pulmonary function, increased susceptibility to respiratory infections, and impaired lung development (Pope et al., 2011; Li et al., 2016; Amnuaylojaroen and Parasin, 2024). Recent evidence highlights a strong correlation between childhood PM exposure and respiratory dysfunction, with children exhibiting diminished lung function, heightened asthma prevalence, and increased respiratory symptoms (Garcia et al., 2021; Zheng et al., 2023). Indeed, the Global Burden of Disease data identifies air pollution as the second largest health risk for children aged 0–14 years worldwide (IHME, 2024).

Residual oil fly ash (ROFA), a byproduct of fossil fuel combustion, is a significant air particulate pollutant commonly found in industrial regions. It has been extensively utilized in toxicological research as a surrogate airborne particle to study physiological and pathological responses to PM in murine models (Dreher et al., 1997; Kodavanti et al., 1998, 2002). Structural lung and extrapulmonary organs injury, marked oxidative stress and increased inflammation are among the effects primarily attributed to ROFA, mainly due to its high concentration of bioavailable transition metals, such as nickel (Ni), vanadium (V), and iron (Fe) (Dreher et al., 1997; Kodavanti et al., 2002; Magnani et al., 2011; Knuckles et al., 2013; Orona et al., 2020)

Studies examining ROFA exposure through intratracheal or intranasal instillation and aerosol inhalation have demonstrated significant functional and structural alterations. Among these administration routes, intranasal instillation offers several advantages, including being painless, non-invasive, cost-effective, and practical, with a rapid onset of action. This route is an effective technique commonly used in toxicity studies (Leong et al., 1998; Southam et al., 2002) and is widely recognized as favorable for systemic drug administration in human medicine (Falcone et al., 2014).

Children are particularly susceptible to the adverse effects of PM exposure due to their developing respiratory systems, higher respiratory rates, and immature immune systems. Lung development, a highly regulated process of proliferation, differentiation, and maturation, is particularly vulnerable to environmental insults during early life (Herriges and Morrisey, 2014).

It is clear that all the processes and events involved in the development of the respiratory system are susceptible to perturbation by environmental influences and that oxidative stress plays a well-described role in mediating PM toxicity. In fact, the oxidative and pro-inflammatory responses induced after PM exposure have also been proposed as underlying mechanisms of cardiometabolic and hepatic disorders (Pope et al., 2004, 2016; Rao et al., 2018; Xu et al., 2019).

Among the target organs affected by PM, the liver and kidneys, key excretory organs, are crucial in detoxifying xenobiotics and systemic homeostasis (Barouki et al., 2023). Exposure to PM could potentially impact these organs in two ways: first, by directly influencing their role in detoxifying xenobiotics absorbed from PM, and second, by causing indirect effects on liver and kidney cells due to inhaled PM.

The liver metabolizes xenobiotics and filters toxins from the blood, processes that can be disrupted by PM-induced oxidative stress and systemic inflammation. In fact, PM exposure has been implicated in exacerbating liver conditions, including diseases such as steatosis, fibrosis and even cancer (Kim et al., 2014; Deng et al., 2017; Xiao et al., 2024).

As a metabolic organ responsible for maintaining the fluid and acid-base balance, the kidney's filtration function makes it vulnerable to environmental pollutants (Xu et al., 2018). Long-term exposure studies have shown an association between PM and a decline in kidney function over time (Shubham et al., 2022), which may be reflected in a reduced glomerular filtration rate (Troost et al., 2024) and increased risk of kidney damage and dysfunction (Aztatzi-Aguilar et al., 2016; Chenxu et al., 2018).

Malnutrition exacerbates the health risks associated with PM exposure, particularly in children. Adequate nutrition plays a crucial role in normal organ development, immune function, and resistance to environmental stressors. Nutritional deficiencies may alter normal lung growth, increase oxidative stress and inflammation, compounding the effects of PM exposure (Fandiño et al., 2019; Stocks et al., 2013; Romieu et al., 2002). Children hospitalized for severe malnutrition usually present their liver and kidneys compromised, with structural and functional changes such as electrolyte disturbances, increased oxidative stress, hepatic steatosis and hypoalbuminemia (Leite et al., 2013; McClain et al., 2017; Parenti et al., 2021).

Early-life factors such as nutrition, coupled with environmental elements like air pollution, could play a role in adversely impacting lung, liver and kidneys development and function. In fact, despite the well-documented systemic effects of PM exposure, little is known about its specific impact on the respiratory, hepatic, and renal systems, especially under conditions of undernutrition. Addressing this gap is critical for understanding the combined health risks in vulnerable populations.

In this context, this study investigates the effects of 4-week Residual Oil Fly Ash (ROFA) exposure on lungs, liver, and kidneys in young rats within a growth-restricted nutrition (NGR) framework, aiming to elucidate the interplay between PM exposure and malnutrition on excretory organ health.

2. Materials and methods

2.1. Animal care

Wistar rats (male, 21–23 days old) were bred at the facility of the School of Pharmacy and Biochemistry, University of Buenos Aires, Argentina. Animals were housed at the animal facility at School of Dentistry of the University of Buenos Aires according to institutional guidelines and kept under standard laboratory conditions (light-dark cycle 12:12h, 21 ± 1 °C and 50–60% relative humidity). Animals were fed a standard diet (Purina chow) of the following composition (g/100g): protein, 22.7; lipids, 7.09; fiber, 6.0; Ca, 1.3; P, 0.8; ashes, 6.5; water, 7.96 and dextrin up to 100g. Animal care and experimental procedures were performed according to the National Institutes of Health Guidelines for the Care and Use of Laboratory Animals (National Research Council-US, 2011) in compliance with Argentinean law and in accordance with the "Principles of Laboratory Animal Care" guidelines and approved by the University of Buenos Aires Ethics Committee, according to the Principles of Laboratory Animal Care (NIH 2 publication number 85–23, revised 1985, 3 http://grants1.nih.gov/grants/olaw/references/phspol.htm).

2.2. ROFA morpho-chemical characterization

ROFA was collected from Boston Edison Co., Mystic Power Plant, Mystic, CT, USA, and kindly provided by Dr. J. Godleski (Harvard School of Public Health, MA, USA). ROFA was previously morphologically and chemically characterized by SEM and EDX (Ghio et al., 2002; Ferraro et al., 2011; Kurtz et al. 2024a, 2024b).

2.3. ROFA exposure and nutritional experimental design

Rats were randomly divided into 2 groups (n = 14/group): control (C) and nutritional growth retardation (NGR). Control rats were fed *ad libitum* with a standard diet, and NGR rats were fed 80% of the amount of food consumed by controls (Lezón et al., 2009; Kurtz et al., 2018, 2024a, 2024b). The food amount was corrected by body weight (food intake in grams per 100 g body weight per day), as can be observed in Table 1. We selected this 20% restricted balanced diet for a 28-day period to model suboptimal nutrition, based on clinical pediatric findings (Lifshitz and Moses, 1988, 1989). This approach closely mirrors the inadequate nutritional intake observed in children consuming inappropriate diets

Table 1
Food consumption during the 4-week experimental protocol.

Food consumption (g/100g BW/day)				
Day	Control	ROFA	NGR	NGR + ROFA
1	15	15	12	12
3	15	15,4	12	12,3
5	16,3	15	13	12
8	13	14,7	10,4	11,8
10	12	13,9	9,4	11,2
12	12	12	9,6	9,6
15	11,4	11,7	9,1	9,4
17	10,7	11	8,6	8,8
19	10,5	10	8,4	8
22	9,5	9,5	7,6	7,6
24	8,9	9	7,1	7,2
26	9,2	9,1	7,4	7,3
29	9,1	9,2	7,3	7,4

Changes along time of food consumption for the dietary control groups and the calculated amount of food given to NGR groups (80% from each control).

that provide insufficient total energy to sustain normal growth and weight gain.

In our study, rats subjected to this type of chronic suboptimal nutrition exhibited a reduced body mass growth rate. Table 2 shows the mean body weight progression of each group, a critical indicator of animal health. By the second weighing (day 3), statistically significant differences ($p < 0.05$) were observed between the control and NGR groups. This difference increased from day 5 onward ($p < 0.001$) and remained constant until the end of the experiment.

Over a 4-week period, the animals were exposed intranasally to ROFA (0.17 mg/kg body weight) or vehicle (sterile PBS) 3 times per week, resulting in four experimental groups: control (C, n = 5–7), control ROFA exposed (ROFA, n = 5–7), undernourished (NGR, n = 5–7), and undernourished ROFA exposed (NGR + ROFA, n = 5–7), as seen in Fig. 1. It has to be pointed out that intranasal instillation is an effective, simple, painless and non-invasive technique commonly used in toxicity studies (Leong et al., 1998; Southam et al., 2002) and that the selection of the ROFA dose was based upon previous studies (Ostachuk et al., 2008; Ferraro et al., 2011).

2.4. Tissue collection

At the end of the 4-week period of dietary and ROFA exposure, the animals were anesthetized and euthanized employing ketamine 0.2 ml/100g BW and xylazine 0.05/100g BW. Blood samples were collected from all animals in order to perform the serological assays and organs were excised and employed for the histological, biochemical and molecular assays. For biochemical purposes the lungs and extrapulmonary organs (liver and kidneys) from 3 to 5 animals per group were excised and stored at −70 °C until analysis. On the other hand, for the histological and histomorphometrical analysis, lung, liver, and kidney samples (target tissues) from 3 to 4 animals per group were fixed in buffered formalin (10%), dehydrated in alcohol and embedded in paraffin.

Table 2
Body weight during the 4-week experimental protocol.

Body weight during the experiment (g)				
Day	Control	ROFA	NGR	NGR + ROFA
1	64,5 ± 2,1	65,2 ± 2,2	67,0 ± 2,5	66,1 ± 2,4
3	75,5 ± 3,2	74,2 ± 3,4	70,3 ± 2,1*	71,0 ± 2,3*
5	82,8 ± 2,9	80,8 ± 3,6	72,8 ± 3,2***	71,0 ± 3,9***
8	102,5 ± 4,4	98,0 ± 4,0	77,2 ± 2,9***	75,1 ± 2,7***
10	124,3 ± 3,9	120,7 ± 3,7	95,5 ± 2,8***	96,7 ± 3,0***
12	140,8 ± 4,1	141,7 ± 3,9	98,4 ± 3,1***	97,1 ± 2,8***
15	159,2 ± 6,4	157,5 ± 5,4	105,4 ± 3,7***	104,0 ± 3,5***
17	181,0 ± 7,7	182,5 ± 6,7	102,0 ± 3,2***	106,2 ± 4,1***
19	200,8 ± 6,5	198,7 ± 7,4	114,2 ± 4,2***	110,4 ± 3,7***
22	220,2 ± 7,2	218,2 ± 7,9	119,2 ± 4,5***	118,5 ± 4,2***
24	230,3 ± 8,1	238,7 ± 8,7	123,0 ± 4,1***	122,2 ± 4,5***
26	247,3 ± 8,4	250,3 ± 7,0	126,2 ± 5,1***	125,7 ± 4,7***
29	270,3 ± 7,9	274,5 ± 8,1	130,6 ± 4,9***	129,3 ± 5,6***

Changes along time after weaning in body weight for the four experimental groups. Values are expressed as mean ± SD from one representative experiment conducted with 6 animal per group (n = 6), One way ANOVA and Bonferroni post-hoc test was performed. *$p < 0.05$, ***$p < 0.001$.

2.5. Histological and Histomorphometrical Evaluation

Histological sections of 5–7 μm thickness from lungs, liver and kidneys were cut with a Reichert-Jung micrometer (Nossloch, Germany), deparaffinized, rehydrated and stained for light microscopy. All pathological changes on the target organs were assessed using Hematoxylin-Eosin (HE) and Periodic Acid Schiff (PAS) staining. Lung samples were also stained with Mallory's trichome for collagen observation, orcein for elastic fibers and toluidine blue stain for mastocyte identification (Sridharan and Shankar, 2012). All samples were observed and photographed under high resolution light-field microscope (Axioskop 2; Carl Zeiss, Jena, Germany) and a digital camera (Nikon CoolPix 12 Mp, Japan).

Lung (H&E or toluidine blue) and kidney (PAS) microphotographs were employed to perform histomorphometrical analysis using an image processing software (Image J 1.54f, National Institutes of Health, USA). Three parameters were analyzed in H&E staining micrographs to evaluate lung tissue structure: percentage of alveolar airspace (%), the number of alveoli per total area (N/mm^2 total area), and the alveolar size distribution. In Toluidine blue staining the number of mastocytes per connective tissue area (N/mm^2) was also evaluated. In kidney, Bowman's space area (mm^2) was measured to evaluate filtration apparatus.

2.6. Serological determinations

Biochemical analysis was performed in serum samples collected from the four experimental groups. Briefly, blood was obtained by cardiac puncture and serum was obtained after blood centrifugation at 13800*g* for 10 min. Total cholesterol, HDL-cholesterol, calcium, phosphorus, urea, as well as alanine aminotransferase (ALT) and aspartate aminotransferase (AST) activities were measured by standardized methods (Roche Diagnostics, Germany) in a COBAS C501 autoanalyzer (Roche Diagnostics GmbH, Germany). Non HDL-cholesterol was calculated as total cholesterol minus HDL cholesterol.

Lipoprotein-associated antioxidant capacity was evaluated using paraoxonase 1 (PON-1) with two different substrates: paraoxon (Sigma-Aldrich Inc., USA; PON-1 activity) and phenylacetate (Sigma-Aldrich Inc., USA; ARE activity) as described by Furlong et al. (1989).

Lp-PLA2 activity was measured employing a previously described colorimetric method (Cerelli et al., 2016).

2.7. Oxidative metabolism

Oxidative metabolism (antioxidant enzymes and lipoperoxidation) was evaluated in organ homogenates as described by Llesuy et al. (1994). Briefly, organs were homogenized in PBS (pH 7.4) at 4 °C (1:5 w/v), the suspension was centrifuged at 6000×*g* for 10 min at 4 °C to remove cell debris, the pellet was discarded and the supernatant was used as "homogenate". We assessed the activity of catalase (CAT) and superoxide dismutase (SOD) antioxidant enzymes, as well as membrane lipoperoxidation using TBARS, in the lungs, liver, and kidneys.

2.7.1. Catalase (CAT) and Superoxide dismutase (SOD) antioxidant enzymes activities

Tissue homogenates were used for antioxidant activity determinations. The activity of CAT was assessed following Maehly and Chance (1954). Rates were calculated as the change in optical density of

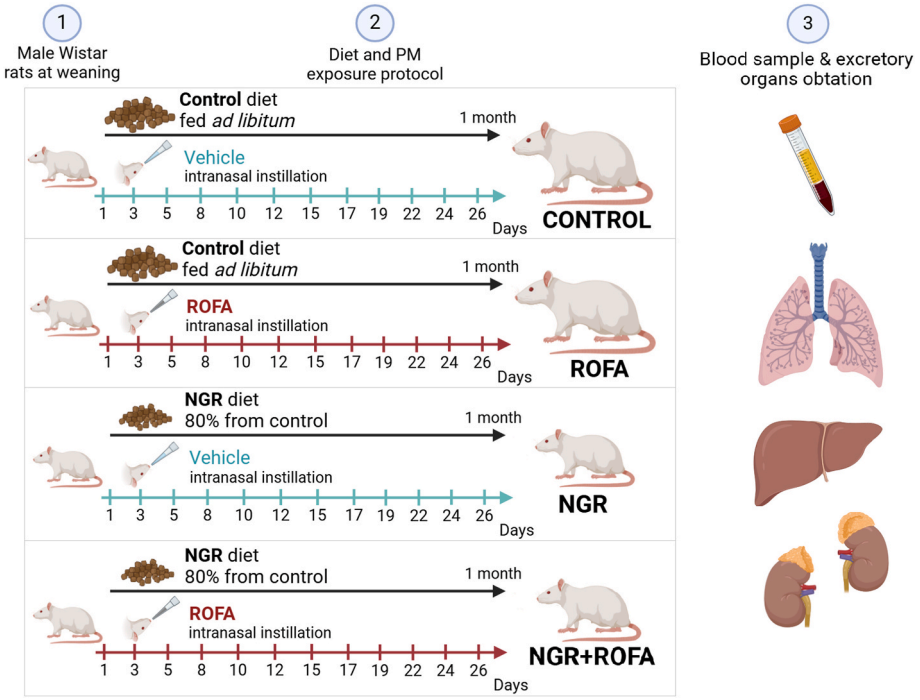

Fig. 1. Nutritional Animal Model and PM Exposure Experimental Design.
Wistar rats were randomized in two groups regarding food intake 1) CONTROL: food intake *ad libitum* or 2) NGR: 80% of the amount of food consumed by control. Simultaneously, each of these dietary groups were intranasally instilled 3 times per week either with ROFA (0.17 mg/kg BW) or it's vehicle (PBS), creating 4 groups: Control, ROFA, NGR, NGR + ROFA. After 24 hs. from the last PM exposure, blood samples were obtained and lungs, liver and kidneys were excised for histological and biochemical analyses.

the assay mixture/min/mg protein. SOD activity was assayed by the method of Misra and Fridovich (1972) and is expressed as SOD units/mg protein. One unit of SOD was defined as enzyme amount producing 50% inhibition epinephrine autoxidation.

2.7.2. *Thiobarbituric acid reactive substances (TBARS)*

Lipid peroxidation was determined spectrophotometrically in tissue homogenates by TBARS, as described by Yagi (1976). Briefly, the homogenate was added with trichloroacetic acid (40% w/v) and centrifuged at 1000×*g* for 10 min. The supernatant was added with an equal volume of thiobarbituric acid (46 mM) (Sigma-Aldrich Co.), and the solution was heated at 95 °C for 15 min. Then, samples were cooled and quantified spectrophotometrically at 535 nm. Malondialdehyde (Sigma-Aldrich Inc., USA) was used as a standard. Results are expressed as nmol TBARS/mg protein.

2.8. *Protein determination*

Proteins were measured by the method of Bradford (1976) using bovine serum albumin as the standard.

2.9. *Cytokine production*

Total organ RNA was extracted using Trizol reagent following the manufacturer's instructions (Life Technologies, Inc.-BRL, Grand Island, NY). The reverse transcription was performed using 2 or 4 μg of total RNA. The cDNAs generated was further amplified by PCR under optimized conditions using the primer pairs listed below. In this study, we analyzed the expression of IL-6, a pro-inflammatory marker, and IL-10, an anti-inflammatory marker, in the lungs, liver and kidneys.

IL-6: Forward, 5′-GACAAAGCCAGAGTCCTTCA-3′, Reverse, 5′-ACTAGGTTTGCCGAGTAGAC-3'. IL-10: Forward, 5' -AGGGTTACTTGGGTTGCC-3′, Reverse, 5′-GGGTCTTCAGCTTCTCTCC-3'. GAPDH (glyceraldehyde 3-phosphate dehydrogenase): Forward: 5′-ACCCAGAAGACTGTG GAT GG-3′, Reverse: 5′-CACATTGGGGGTAGGAACAC-3.

The number of cycles used was optimized for each mRNA to fall within the linear range of PCR amplification. PCR products were redissolved in a 1% (wt/vol.) agarose gel. The gel images were acquired with the GelPro analyzer (IPS, North Reading, MA). The levels of mRNA were quantified using a computer-assisted image analyzer (ImageQuant 5.2) and the PCR results for each sample were normalized with GAPDH mRNA as an internal control.

2.10. *Statistical analysis*

Results were expressed as mean values ± standard error of the mean (SEM), representing the mean of 4 independent experiments. Statistical analysis was performed using two-way ANOVA, followed by Bonferroni's post-hoc test, with statistical significance set at $p < 0.05$.

3. Results

3.1. *ROFA morpho-chemical characterization*

We analyzed the size, morphology, and chemical composition of Residual Oil Fly Ash (ROFA) using scanning electron microscopy (SEM) coupled with energy-dispersive X-ray spectroscopy (EDX). The results are consistent with previous findings from our group and others, highlighting morphological heterogeneity in shape and size (Ghio et al., 2002; Ferraro et al., 2011; Kurtz et al. 2024a, 2024b). A SEM microphotograph of ROFA particles (Fig. 2) demonstrate a wide size range, primarily spanning from 3.6 μm to 0.49 μm, indicating significant dimensional variability. This distribution includes both coarse particles (PM10) and fine particles (PM2.5), which exhibit distinct behaviors and health implications. Elemental composition analysis (Table 3) reveals a high content of transition metals, including vanadium, nickel, and iron, along with trace amounts of barium, embedded in a rich-aluminum

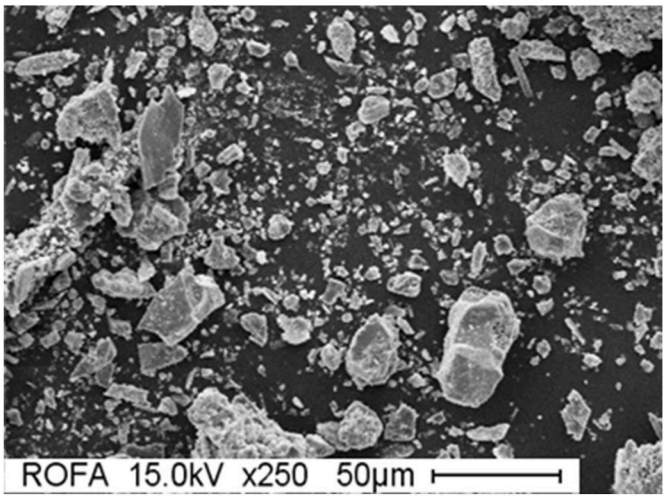

Fig. 2. SEM photomicrograph of ROFA particles. The particles display a variety of sizes with a mean diameter of 2.06 ± 1.57 µm.

Table 3
ROFA elemental composition. The elemental composition corresponds to a vanadium – rich aluminum silicate particle with high levels of iron and nickel, collected from Mystic Power Plant.

ROFA Elemental Composition		
Element	Wt %	At %
C K	1.60	4.53
O K	16.26	34.64
Na K	04.03	5.98
Mg K	2.63	3.68
Al K	2.67	3.38
Si K	5.11	6.20
K K	0.67	0.59
Ca K	1.50	1.27
Ba L	2.86	0.71
Ti K	0.44	0.31
V K	31.38	20.99
Fe K	7.59	4.63
Ni K	15.71	9.12
Cu K	2.55	1.37
Zn K	4.99	2.60
Total	100.000	100.000

silicate composition.

3.2. Histopathological analysis

3.2.1. The lung

Control lung sections exhibit a typical appearance with normal alveolar structure. In contrast, NGR rat lungs display thinner alveolar walls where growing septa are dividing the larger compartments (Fig. 3). ROFA exposure induces the recruitment of inflammatory cells (macrophages, polymorphonuclear, and lymphocytes) in both control and NGR animals therefore, leading to a reduction of the alveolar space compared to their non-exposed counterparts. NGR + ROFA depict a notable vascular congestion increase (Fig. 3 arrows). Furthermore, we investigated the involvement of PM-induced toxic effects in mucus hyperproduction for all animal experimental groups. Compared to control rats, NGR exhibited a decrease in PAS-positive cells in the epithelium from the bronchiolar region as observed by Periodic Acid-Schiff Stain (PAS). On the contrary, in all ROFA-exposed lung rats we found an increase in PAS-positive cells and subepithelial cell infiltration (Fig. 3 insets).

For a more accurate description, we conducted an histomorphometric analysis to quantitate the alveoli airspace, the number of alveoli and the alveolar size distribution. A clear decrease in the percentage of the alveolar space was seen after ROFA exposure for both control and NGR animals (C 55.8 ± 1.8 vs. ROFA 38.7 ± 3.0, $p < 0.01$; NGR 61.3 ± 1.0 vs. NGR + ROFA 44.2 ± 3.3, $p < 0.001$) (Fig. 4A). As seen in Fig. 4B, the number of alveoli per area also diminished after ROFA exposure (C 492 ± 31 *vs.* ROFA 247 ± 10, $p < 0.001$; NGR 481 ± 31 *vs.* NGR + ROFA 302 ± 17, $p < 0.001$). Changes in the alveolar size distribution were observed in ROFA and NGR + ROFA when compared to their counterparts (Fig. 4C). NGR + ROFA exhibit a positively skewed distribution, showing an increase in larger alveolar spaces (Fig. 4C). This experimental group also showed a larger mean alveoli size (1830 ± 378 µm2) when compared to the control and NGR groups (Control = 1255 ± 92, NGR = 1243 ± 93 µm2).

As seen in Fig. 5, Mallory's trichrome stained sections from control animals elicited a continuous well-defined smooth muscle layer, prominently visible under the bronchiolar mucosa, while the NGR group shows a reduction in the thickness of this layer. All animals exposed to ROFA exhibited a notable pattern of discontinuity in the smooth muscle structure and disruption in the elastic fiber network as seen in orcein stained sections (Fig. 5: insets). A marked thickening of the bronchial mucosal layer due to the presence of inflammatory cell infiltrate was also found in ROFA exposed animals (Fig. 5).

Mast's cells metachromatic granules were identified with Toluidine Blue stain (Fig. 6A). Microphotographs of ROFA exposed animals depicted an increase in mast cells. To validate this observation, we quantitate the number of mast cells per area. As expected, after ROFA exposure we found an increase in mast cell number being the difference significative only between control and ROFA groups (Fig. 6B).

3.2.2. The liver

Liver sections from control animals display the typical hexagonal arrangement of hepatic lobules with a central vein and portal tracts at the lobule periphery. In contrast, NGR liver sections exhibit smaller hepatocytes and the presence of some binucleated cells compared to the control group. In the hepatic parenchyma of rats exposed to ROFA, we observed the presence of microvesicles characterized by distended hepatocytes with a foamy cytoplasm and small lipid vesicles 1 µm in diameter, sinusoidal dilation and congestion (Fig. 7). Additionally, both ROFA-exposed groups showed an increase in the number of binucleated hepatocytes (Fig. 7 inset). No vesicles, signs of inflammation or rise in the number of binucleated cells were observed in control animals.

As shown in Fig. 8, ROFA-treated animals displayed a marked increase in PAS-positive hepatocytes. The NGR groups exhibited a patchy distribution of PAS-positive cells, indicating glycogen depletion, particularly near the centrilobular vein-a region with lower oxygenation. It is to note that NGR + ROFA depicted a more accentuated patchy pattern than NGR.

3.2.3. The kidney

Kidney H&E-stained sections from control animals show normal glomerular architecture, no inflammation, no hemorrhage and intact tubular lumen (Fig. 9A). In the ROFA group, we observed hyaline cylinders in the lumen, inflammatory cell infiltration and some focal hemorrhage along with a decrease in the Bowman's space (Fig. 9A). Furthermore, the unnourished animal (NGR and NGR + ROFA) groups exhibit smaller glomeruli with reduced Bowman's space and congested interstitium though the overall renal architecture remains preserved (Fig. 9A). Quantification of Bowman's space area showed a significant decrease in the filtration space in animals exposed to ROFA or to a restricted diet (Fig. 9B). ROFA exposure significantly reduced the Bowman's space with respect to controls (C = 2.15 ± 0.2 vs. ROFA = 1.74 ± 0.2, $p < 0.05$). Malnutrition induced a further reduction (C = 2.15 ± 0.2 vs. NGR = 1.06 ± 0.1 $p < 0.001$) regardless ROFA exposure (NGR = 1.06 ± 0.1 vs. NGR + ROFA = 1.34 ± 0.1, $p > 0.05$).

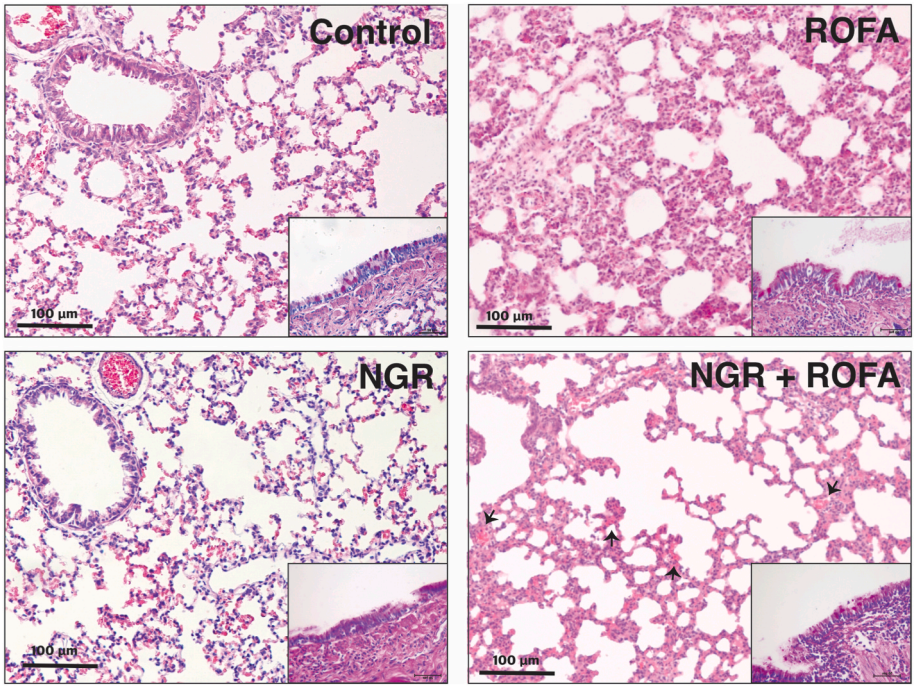

Fig. 3. Lung Sections Stained with Hematoxylin-Eosin (H&E) and Periodic Acid Schiff reaction (PAS).
Representative microphotographs of the lower respiratory tract from the 4 experimental groups. Control lung sections show normal alveoli architecture while NGR display thinner alveolar walls. ROFA exposure induces the recruitment of inflammatory cells leading to reduced airspace compared to their non-exposed counterparts. A notable increase in larger alveolar spaces and vascular congestion (arrows) is observed in NGR + ROFA animals. Original magnification 200X. Insets show PAS-stain lung respiratory epithelium. A clear augmentation in PAS-positive cells and subepithelial lymphoplasmacytic infiltration is evidenced in all ROFA exposed animals. Original magnification 400X.

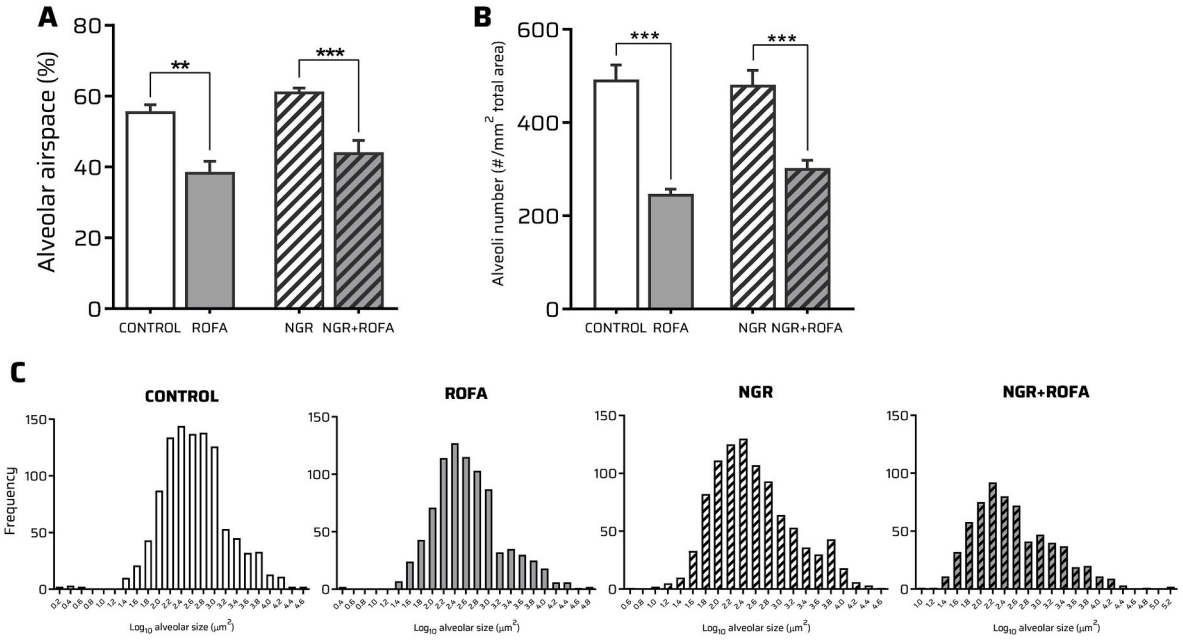

Fig. 4. Histomorphometric Evaluation of the Lung.
A) percentage of alveolar airspace, B) alveoli number and, C) alveolar size distribution for all four experimental groups. Exposure to ROFA induces a significative decrease in alveolar space (4A), alveoli number (4B) and changes in alveolar size distribution (4C).
Results are expressed as mean ± SEM, n = 5–7 animals per group. Two-way ANOVA in conjunction with Bonferroni's post-test were performed, *p < 0.05, **p < 0.01, ***p < 0.001.

3.3. Oxidative metabolism

Air pollution and malnutrition are factors that can adversely affect organ function by disrupting oxidative metabolism thus, we assessed organ antioxidant enzymes activities and lipoperoxidation. As shown in Fig. 10, ROFA-exposed control lungs elicited a significant reduction in CAT activity ($p < 0.05$), while SOD activity showed no differences. In the NGR group, ROFA exposure did not produced changes for any of the

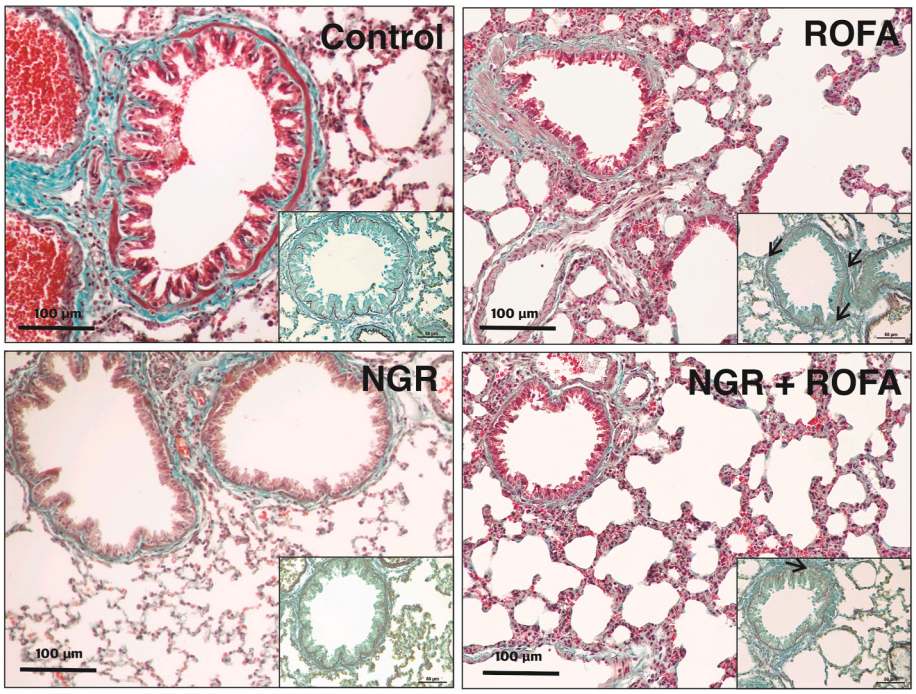

Fig. 5. Lung Sections Stained with Mallory's Trichrome and Orcein.
Representative microphotographs of the lung parenchyma from the 4 experimental groups. Control lung shows a normal continuous smooth muscle layer and collagen tissue in the bronchial mucosa. NGR lung shows a thinner smooth muscle layer while ROFA and NGR + ROFA lung sections show a discontinuous smooth muscle layer. Original magnification 200X. Insets show Orcein lung-stained sections where a clear disorganization of the elastic fiber network for ROFA exposed animals (arrows) is observed. Original magnification 400X.

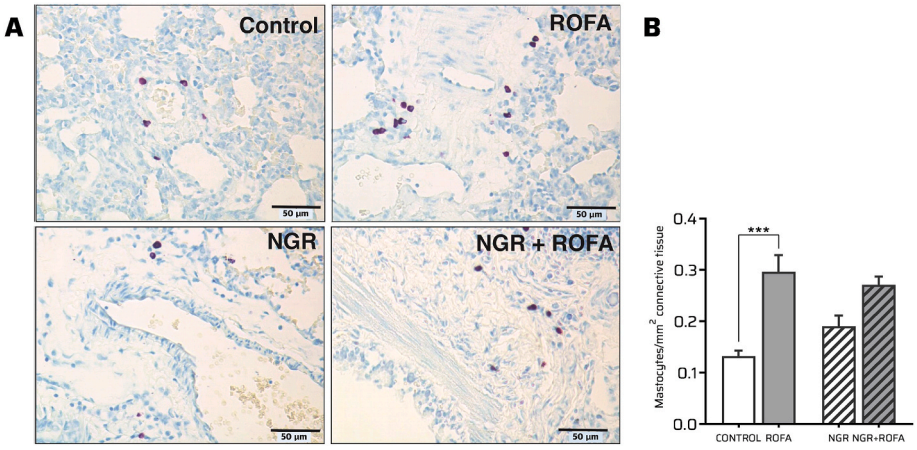

Fig. 6. Qualitative and Quantitative Mast Cells Evaluation in the Lung.
A) Representative microphotographs of lung parenchyma from the 4 experimental groups stained with Toluidine Blue. ROFA exposure shows a notable increase in mast cell number. Original magnification 400X. B) Histogram showing mast cell number per area. A significant increase is observed in control animals exposed to ROFA. Results are expressed as mean ± SEM, n = 5–7 animals per group. Two-way ANOVA in conjunction with Bonferroni's post-test was performed, ***$p < 0.001$. (For interpretation of the references to color in this figure legend, the reader is referred to the Web version of this article.)

antioxidant enzymes assayed. Significant differences in CAT ($p < 0.05$) and SOD ($p < 0.001$) activities were observed in the NGR group compared to the control group, likely indicating diet-induced effects. Both the control group and the NGR group exhibited an increase in lipoperoxidation after ROFA exposure, being this change statistically significant in the NGR + ROFA group ($p < 0.05$) when compared to the NGR group. In the liver, CAT antioxidant enzyme activity remained unchanged across all experimental groups. SOD activity did not change following ROFA exposure in the control group, while in the NGR group a significant increase was observed. It is to note that NGR animals showed basal lower SOD activity level. However, TBARS levels remained stable in both groups, irrespective of ROFA exposure. Following ROFA exposure in the kidneys no changes in CAT or SOD antioxidant enzyme activities were observed neither for control nor NGR animals. However, SOD activity in the NGR group was significantly reduced ($p < 0.001$) compared to those in the control group, likely due to differences in nutritional status. Neither ROFA exposure nor diet had any effect on lipoperoxidation levels.

3.4. Cytokine production

In the lungs, basal IL-6 expression was higher in the NGR animals

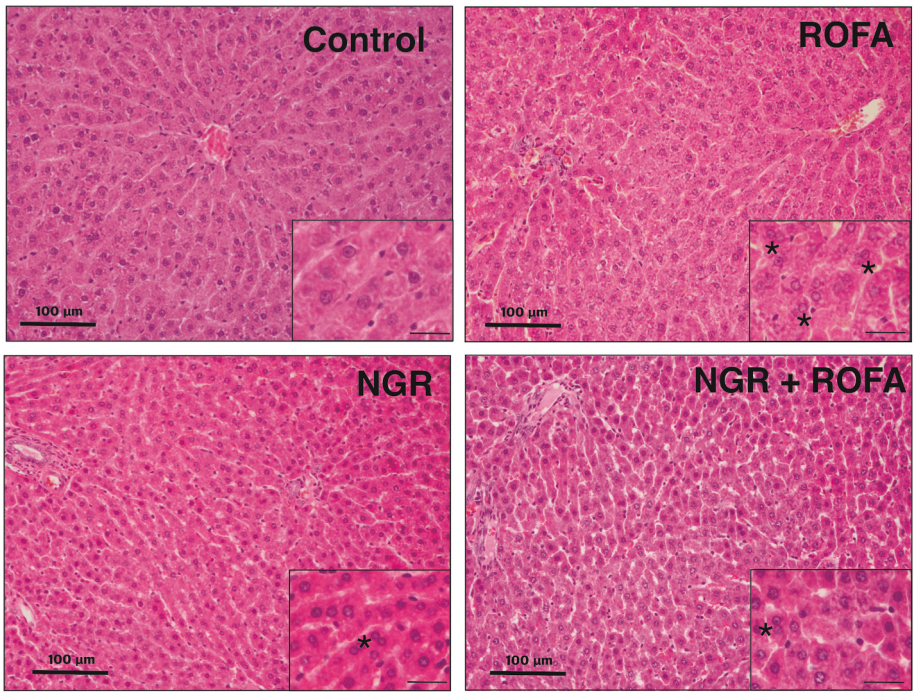

Fig. 7. Liver Sections Stained with Hematoxylin-Eosin (H&E).
Representative microphotographs of liver sections from the 4 experimental groups. The control group displays normal, well-preserved liver architecture with no signs of inflammation, steatosis, or fibrosis. NGR liver sections show smaller hepatocytes, with some binucleated cells (asterisks). ROFA and NGR + ROFA liver sections exhibit microvesicles and an increase in binucleated hepatocytes (asterisks). H&E, Original magnification 200X, inset: 400X. inset scale bar represents 25 µm.

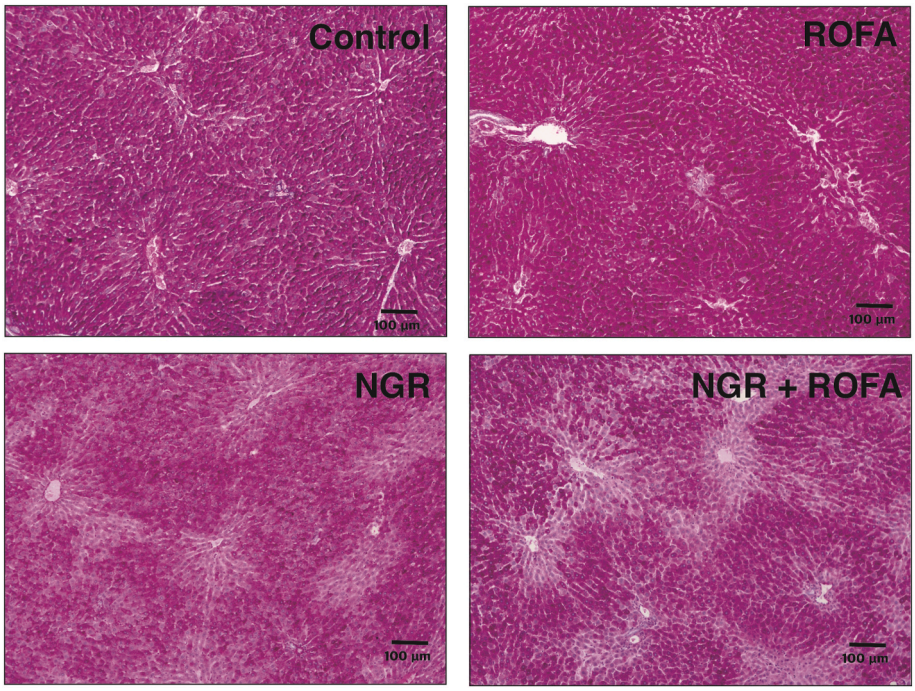

Fig. 8. Periodic Acid Schiff Reaction (PAS)-stained Liver Sections.
Representative microphotographs from the 4 experimental groups. A homogeneous and stronger PAS reaction intensity is shown in hepatocytes from ROFA exposed animals, while NGR and NGR + ROFA groups exhibit a patchy pattern of PAS-positive cells. Original magnification 100X.

compared to the control animals ($p < 0.01$). As shown in Fig. 11, treatment with ROFA significantly increased IL-6 levels only in the control group ($p < 0.01$), with no further effect on the NGR group. The anti-inflammatory cytokine IL-10 expression mirrored that of IL-6. When analyzing cytokine status in the liver, ROFA exposure significantly increased IL-6 levels ($p < 0.001$) and IL-10 levels ($p < 0.05$) with respect to the control group. NGR basal IL-6 and IL-10 expressions were significantly higher when compared to the control group ($p < 0.001$) being unchanged by ROFA exposure. In the kidney, following ROFA treatment, a significant increase in IL-6 levels was observed only

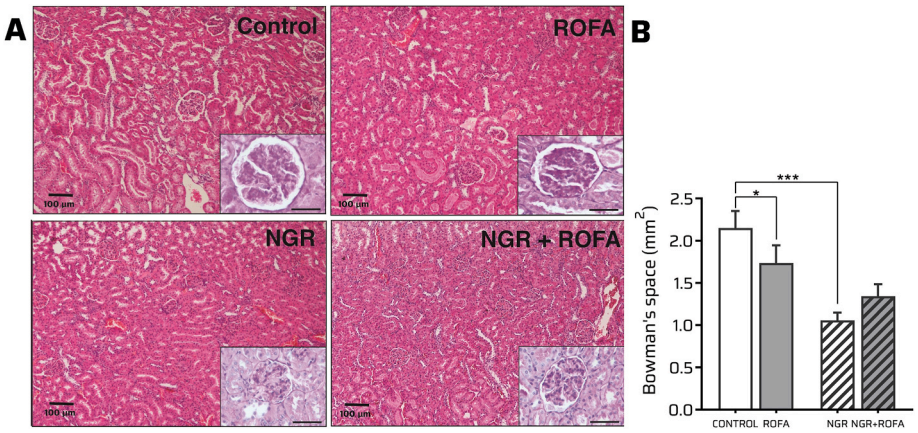

Fig. 9. Qualitative and Quantitative Kidney's Parenchyma Analyses.
A) Representative microphotographs of the kidneys from the 4 experimental groups stained with Hematoxylin-Eosin (H&E) and Periodic Acid-Schiff reaction (PAS) (inset). Control sections display normal kidney architecture while ROFA show hyaline cylinders, inflammatory cell infiltration, focal hemorrhage and reduced Bowman's space. NGR and NGR + ROFA present smaller glomeruli and narrower Bowman's spaces compared to controls. H&E, Original magnification 100X, PAS inset: 400X. Inset scale bar represents 50 µm. B) Bowman's space area histomorphometrical quantitation. A significant decrease in the filtration space is observed in animals exposed to ROFA or subjected to a restricted diet compared to the control group. Results are expressed as mean ± SEM, n = 5–7 animals per group. Two-way ANOVA in conjunction with Bonferroni's post-test were performed, *p < 0.05, ***p<0.001.

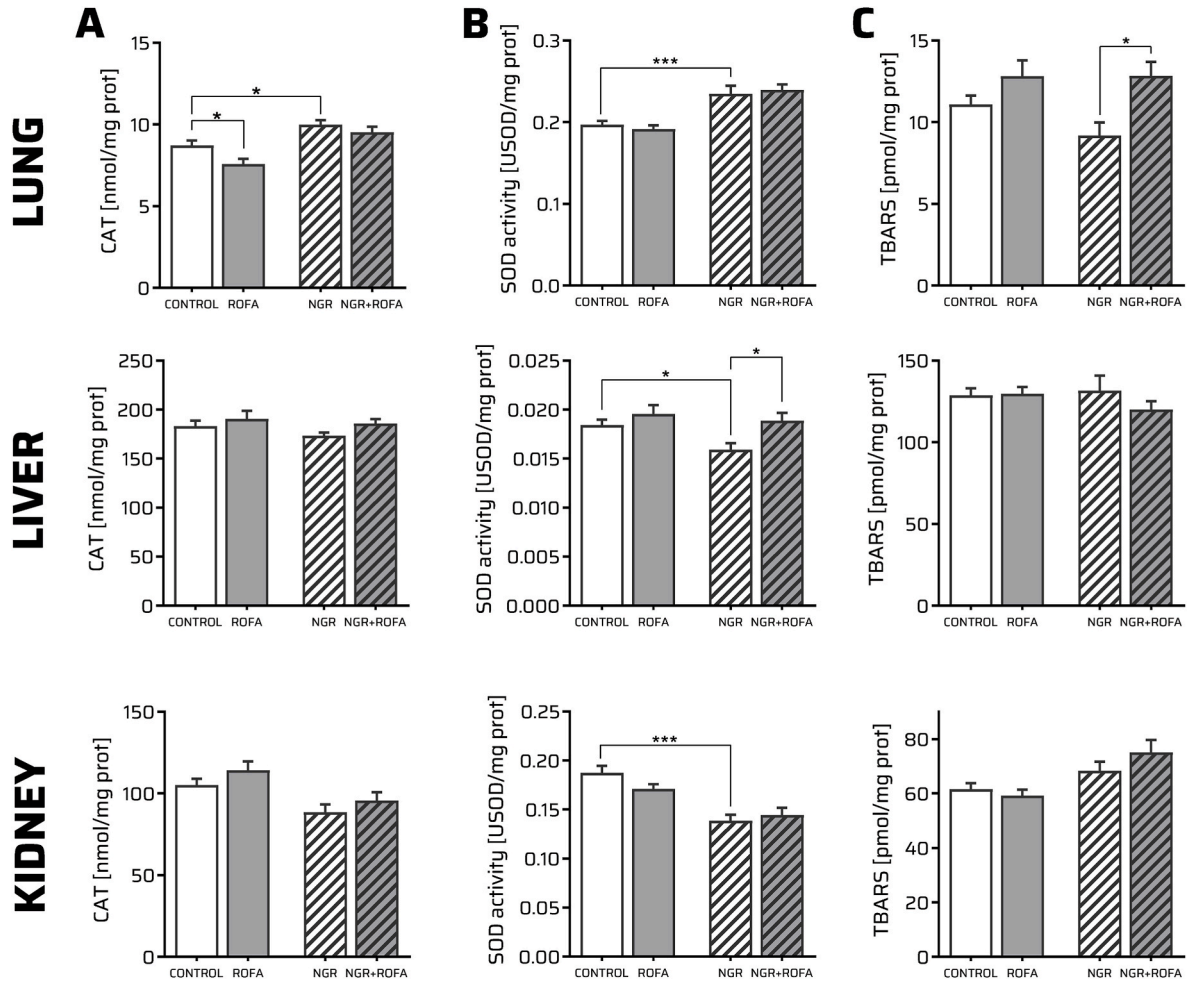

Fig. 10. Oxidative Metabolism in the Lung, Liver and Kidney.
A) Catalase activity, B) Superoxide dismutase activity and, C) Lipoperoxidation. Results are expressed as mean ± SEM, n = 5–7 animals per group. Two-way ANOVA in conjunction with Bonferroni's post-test were performed. *p < 0.05, ***p < 0.001.

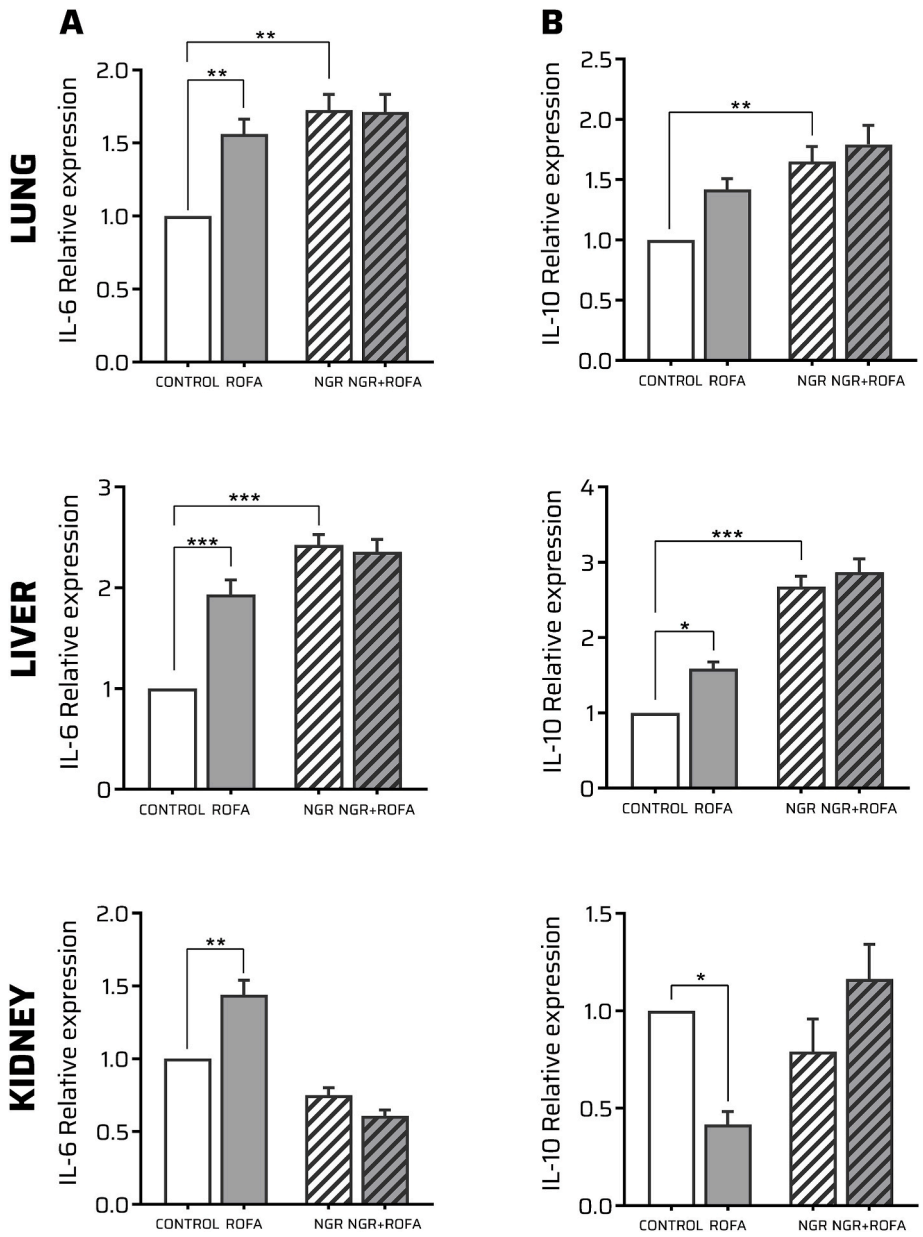

Fig. 11. Cytokine Expression in Lung, Liver and Kidney.
A) IL-6 relative expression and B) IL-10 relative expression. ROFA exposure induced changes in cytokine expression only in the control group. NGR showed higher basal levels for both cytokines with respect to control in lung and liver. Results are expressed as mean ± SEM, n = 5–7 animals per group. Two-way ANOVA in conjunction with Bonferroni's post-test were performed. *p < 0.05, **p < 0,01, ***p < 0.001.

in the control group and, on the contrary, IL-10 expression significantly decreased ($p < 0.05$) (Fig. 11). Interleukins 6 and 10 production showed neither differences between control and NGR groups nor between the NGR + ROFA and NGR groups.

3.5. Serological determinations

As seen in Table 4, total cholesterol, and Non-HDL-C levels are increased in ROFA exposed animals whereas these two parameters along with HDL-C are augmented in NGR and NGR + ROFA animals with respect to controls. Hepatic physiological markers showed that ROFA exposed animals presented higher ALT and AST activities while, NGR showed lower ALT. As functional kidney and metabolic marker, a significant reduction in urea concentration was found in NGR animals with respect to the control group. Regarding lipoprotein oxidative metabolism, the activities of the antioxidant enzymes PON-1 ($p < 0.001$), ARE ($p < 0.001$), and Lp-PLA2 ($p < 0.01$) were significantly reduced compared to control animals.

4. Discussion

Exposure to environmental pollutants together with diet and lifestyle can contribute to the progression of metabolic disruption, however, the mechanisms involved are not completely understood. Therefore, to better understand the impact of these two stressors on children, this study uses ROFA, an industrial PM, characterized by its high content in metallic traces such as the heavy metal vanadium (Ferraro et al., 2011; Orona et al., 2014; Kurtz et al., 2024a, 2024b) and an animal model of chronic undernutrition (Lezón et al., 2009; Kurtz et al., 2018).

Chronic exposure to noxious gases, PM and/or the mixture of gases and particles (Zhou et al., 2014; Li et al., 2018; Jiang et al., 2020) was particularly associated with lung diseases. Children, in particular, have

Table 4
Serum biochemical parameters.

Serum parameters	CONTROL	ROFA	NGR	NGR + ROFA
Total cholesterol (mg/dL)	65.2 ± 1.8	72.7 ± 2.2*	85.2 ± 0.9###	81.3 ± 2.5
HDL-C (mg/dL)	27.4 ± 0.3	28.7 ± 0.3	32.4 ± 0.7###	31.2 ± 0.6
Non-HDL-C (mg/dL)	36.7 ± 1.3	43.9 ± 2.2**	49.6 ± 0.7###	49.3 ± 2.1
Calcium (mg/dL)	10.2 ± 0.1	10.8 ± 0.2	10.6 ± 0.3	10.9 ± 0.3
Phosphorus (mg/dL)	9.3 ± 0.3	10.0 ± 0.4	9.1 ± 0.4	10.1 ± 0.6
ALT (U/L)	44.5 ± 0.9	49.4 ± 1.3*	38.8 ± 1.6##	42.2 ± 1.2
AST (U/L)	77.7 ± 1.3	81.6 ± 1.3*	79.0 ± 0.4	80.3 ± 1.5
Urea (mg/dL)	43.1 ± 1.4	42.5 ± 1.1	28.2 ± 0.2###	26.6 ± 1.5
PON (mmol/mL*min)	258.7 ± 7.6	233.2 ± 9.1	178.3 ± 10.7###	153.0 ± 10.6
ARE (μmol/mL*min)	124.1 ± 2.4	120.7 ± 3.8	89.8 ± 4.2###	89.4 ± 4.4
Lp-PLA2 (μmol/mL*min)	2.76 ± 0.07	2.81 ± 0.07	2.36 ± 0.12##	2.59 ± 0.14

Serum biochemical parameters evaluated in all 4 experimental groups. HDL, high density lipoprotein; ALT, alanine aminotransferase; AST, aspartate aminotransferase; PON, paraoxonase; ARE, arylesterase; $LpPLA_2$, lipoprotein-associated phospholipase A_2. Results are expressed as mean ± SEM, n = 5–7 animals per group. Two-way ANOVA in conjunction with Bonferroni's post-test were performed. Asterisks represent statistically significant difference between control and ROFA groups or NGR and NGR + ROFA groups (*p < 0.05, **p < 0,01). Numerals represent statistically significant difference between the control and the NGR groups (##p < 0,01 and ###p < 0,001).

more permeable respiratory systems, higher ventilation rates, and less mature immune systems, making them less effective at eliminating and detoxifying inhaled air particles. The total alveolar airspace, as well as the number and size of alveoli in the lung, are key structural determinants of respiratory parenchymal architecture and, consequently, essential for proper lung function. Our study revealed that both control and NGR animals exposed to ROFA exhibited lung alterations, including a significant reduction in both alveolar airspace and alveolar number, with changes in alveolar size distribution that were more pronounced in the NGR + ROFA group. Furthermore, we have identified a clear disruption of the smooth muscle layer in both control and NGR animals upon exposure to ROFA, that along with the lumen area reduction could potentially lead to a decrease in gas-exchange surface area and the respiratory function, contributing to various lung pathologies (Thurlbeck and Müller, 1994; Pauwels et al., 2001; Stephens, 2001; Doeing and Solway, 2013; Cieri, 2019).

Mast cells, located at the host-environment interface, recognize harmful antigens and are involved in chronic allergic, inflammatory, autoimmune diseases and cancer (Rao and Brown, 2008; Tsai et al., 2011). Chronic exposure to environmental air pollutants, including PM, can activate mast cells, potentially leading to inflammation in respiratory tissue (Diaz-Sanchez et al., 2000; Yang et al., 2022). In agreement, we observed in ROFA-exposed animals an evident increase in the number of mast cells in the lung parenchyma, indicating an undergoing chronic inflammatory process. Histamine from mast cells triggers proinflammatory cytokines (IL-6, IL-8) and anti-atherogenic eicosanoids (PGI2, PGE2) (Li et al., 2001). In our study, ROFA exposure increased mast cells and IL-6 only in the control group. It's important to highlight that the NGR group already exhibited a higher number of mast cells and basal IL-6 levels compared to the control group, likely due to a baseline state of stress and chronic inflammation. Our findings are consistent with epidemiological evidence showing that ultrafine PM2.5 exposure raises IL-6 respiratory and cardiovascular disease in patients (Schneider et al., 2010; Cliff et al., 2016; Manzano-León et al., 2016). Interestingly, in the lungs of ROFA-exposed animals, the anti-inflammatory cytokine IL-10 is augmented in an apparent effort to counterbalance the inflammatory response.

Research in mice shows that PM exposure can lead to the nonalcoholic fatty liver disease (NAFLD), the most common chronic liver disease, which may progress to a non-alcoholic steatohepatitis (NASH)-like state. While NAFLD is often linked to obesity and aging, it can also result from nutritional deficits, impacting undernourished children. In this context, severe undernutrition has also been shown to promote fatty liver through impaired lipid metabolism (Li et al., 2015; van Zutphen et al., 2016). Recent studies estimate NAFLD affects 3–12% of children (Bush et al., 2017) and that up to 30% of NAFLD cases may progress to NASH, characterized by hepatocellular ballooning, inflammation and fibrosis (Takahashi and Fukusato, 2014). In our study, ROFA exposure caused liver lesions with micro and macrovesicles, typical of NASH. This aligns with findings from Maglione et al. (2020) and Orona et al. (2020), who reported hepatic steatosis and increased reactive oxygen species (ROS) in young mice exposed to urban PM. Of greater interest is the fact that similar liver alterations have been observed in petrochemical workers exposed to toxins (Cotrim et al., 1999). In the ROFA and NGR + ROFA liver sections, microvesicles suggest the presence of glycogen storage disease (glycogenosis) or microvesicular steatosis. Furthermore, in all ROFA-exposed animals we found an increase of binucleated hepatocytes possibly indicating injury response with nuclear division but incomplete cytoplasmic separation.

Nephrotoxic compounds affect the kidney's functional unit, mainly the glomeruli and the proximal tubules. Accordingly, reduction in the glomerular filtration rate has been reported after chronic and subchronic exposure to PM (Aztatzi-Aguilar et al., 2016) and prolonged exposure to air pollution was directly associated to a higher risk of developing acute kidney injury and its related death (Liu et al., 2024). PM chemically characterized by the presence of metallic traces constitute an important exogenous source of ROS, which can initiate molecular mechanisms leading to oxidative damage upon interaction with tissues. Oxidative stress induces lipid peroxidation in cell membranes, triggering cell damage and contributing to the development of various diseases. PM containing metal traces is a significant source of ROS, which cause oxidative damage in tissues, further exacerbating disease progression (Lee et al., 2017; Xu F. et al., 2020). In this sense, exposure to heavy metals has been associated with chronic kidney disease (Jha et al., 2013). In this study, we observed changes in kidney histology, particularly in the glomeruli and proximal tubules of animals exposed to ROFA. The morphological alterations observed may be associated with glomerular filtration failure and damage to tubular kidney cells which in turn, could potentially be attributed to metallic traces such as vanadium, present in ROFA particles. Vanadium, by triggering ROS, could not only induce an oxidative metabolism imbalance but also initiate a subsequent increase in proinflammatory cytokines. This could partially explain the significant increase in IL-6 observed in the kidneys of control animals exposed to ROFA.

When we analyzed serum parameters, we observed that the animals exposed to ROFA presented higher ALT and AST activities, which is consistent with the aforementioned hepatic alterations observed in this group. In this regard, air pollution is known to induce hepatic inflammation (Paoin et al., 2023). On the contrary, the animals subjected to NGR showed lower ALT thus evidencing the presence of a decreased synthetic capacity of the liver as a result of malnourishment (Siddiqui et al., 2021). Consistently, this group also displayed reduced urea concentration, which could be attributed to a decrease in nitrogen metabolism (Emery, 2005). Regarding lipid parameters, ROFA-exposed

animals showed higher total and non-HDL-cholesterol than controls. This result reflects an increased production of apo B-containing lipoproteins. Indeed, past evidence suggests a link between air pollution and increased production of very low-density lipoproteins in the liver (Zhang et al., 2023). These two parameters together with HDL-C were also increased in animals subjected to NGR compared to those that received a normal diet. This increase would be the result of an increase in cholesterol transport from peripheral tissues to the liver combined with reduced catabolism of apo B-containing lipoproteins rather than an increase in endogenous cholesterol synthesis. As we have proposed earlier, NGR-induced hypoinsulinemia would be responsible for this phenomenon (Lifshitz et al., 2012). PON 1 is an antioxidant enzyme mainly carried by HDL particles in plasma and is mainly responsible for HDL cardioprotective activity (Mahrooz, 2024). Previous studies suggest that undernutrition can affect PON 1 status, limiting its protective capacity. Malnutrition-associated oxidative stress and oxygen radical production would be the mechanism responsible for this alteration (Martin et al., 2023). Indeed, excessive free radical production can overwhelm PON 1, impairing its antioxidant activity. In agreement, Lp-PLA_2 activity, another antioxidant enzyme associated with HDL was also reduced in NGR rats (Brites et al., 2017). These findings suggest that HDL particles would be deteriorated in these animals, losing their cardioprotective function.

This study has certain limitations that should be considered when interpreting the findings. One notable limitation is that our experimental protocol involved a 4-week exposure, which does not mimic the chronic exposure observed in real-world scenarios. In affected populations, prolonged exposure to PM and undernutrition typically occurs over months or years. While our study provides valuable insights into acute biological responses, it may not fully capture the cumulative and long-term effects of chronic exposure. Future research should adopt long-term exposure models to better represent these conditions and evaluate the full extent of associated health risks. Additionally, the PM used in this study, is an industrial pollutant derived from oil combustion. Although ROFA shares some chemical similarities with urban PM, it does not fully replicate the chemical composition, physical properties, or size distribution of PM present in different cities or regions. Thus, incorporating diverse air PM samples in future studies would help better reflect the heterogeneity of urban air pollution and amplify the relevance of our findings.

Nevertheless, we believe that these findings, using an animal model that mirrors developmental stages in rats and humans, may reflect the morpho-functional differences between healthy and undernourished children exposed to air pollution.

5. Conclusion

This study offers a novel and comprehensive morpho-biochemical analysis of the combined effects of PM exposure and malnutrition on the respiratory, hepatic, and renal systems. It underscores the complex interplay between environmental pollutants and nutritional stress in shaping organ function and vulnerability during early development.

Young rats subjected to a restricted diet combined with exposure to ROFA have shown altered morphology and inflammation possibly leading to impaired respiratory function, liver steatosis and glomerular filtration failure. Furthermore, these changes may impair organ function in adulthood, potentially initiating or exacerbating morbidity in susceptible individuals.

ROFA exposure leads to oxidative stress that overwhelms antioxidant defenses and promotes sustained oxidative damage. Additionally, undernutrition primes the inflammatory state by elevating baseline levels of pro-inflammatory cytokines, reducing the ability of malnourished individuals to adequately respond to further insults such as ROFA exposure. Together, these findings indicate that these two stressors had a negative impact on the lungs and excretory organs in young rats, through mechanisms involving oxidative stress and inflammation, with nutritional status influencing a differential physiological response to PM exposure.

CRediT authorship contribution statement

Ivana Masci: Writing – original draft, Investigation, Formal analysis, Data curation. **Carola Bozal:** Writing – original draft, Methodology, Investigation, Formal analysis. **Christian Lezón:** Methodology, Funding acquisition. **Maximiliano Martin:** Investigation, Formal analysis. **Fernando Brites:** Writing – original draft, Investigation, Formal analysis, Data curation. **Julián Bonetto:** Investigation. **Laura Alvarez:** Writing – original draft, Investigation, Funding acquisition, Formal analysis. **Melisa Kurtz:** Writing – review & editing, Writing – original draft, Investigation, Funding acquisition, Formal analysis, Data curation, Conceptualization. **Deborah Tasat:** Writing – review & editing, Writing – original draft, Validation, Methodology, Funding acquisition, Formal analysis, Data curation.

Funding sources

This work was partially supported by the National Agency for the Promotion of Science and Technology, Argentina; contract grant number: PICT 2017-1309 and PICT 2017-4549, Sociedad Argentina de Biología (SAB) Subsidio Eduardo Charreau 2021 (SAB), PIP 2021–2023 Project GI-11220200100397CO, CONICET and UBACyT #20020220400226BA, University of Buenos Aires.

Declaration of competing interest

The authors declare that they have no known competing financial interests or personal relationships that could have appeared to influence the work reported in this paper.

Acknowledgements

The authors would like to thank Ms. Mariela Lacave and Ms. Paula Rocha for their technical assistance.

Data availability

Data will be made available on request.

References

Amnuaylojaroen, T., Parasin, N., 2024. Pathogenesis of $pm_{2.5}$-related disorders in different age groups: children, adults, and the elderly. Epigenomes 8 (2), 13. https://doi.org/10.3390/epigenomes8020013.

Aztatzi-Aguilar, O.G., Uribe-Ramírez, M., Narváez-Morales, J., De Vizcaya-Ruiz, A., Barbier, O., 2016. Early kidney damage induced by subchronic exposure to PM2.5 in rats. Part. Fibre Toxicol. 13 (1), 68. https://doi.org/10.1186/s12989-016-0179-8.

Barouki, R., Samson, M., Blanc, E.B., Colombo, M., Zucman-Rossi, J., Lazaridis, K.N., Miller, G.W., Coumoul, X., 2023. The exposome and liver disease - how environmental factors affect liver health. J. Hepatol. 79 (2), 492–505. https://doi.org/10.1016/j.jhep.2023.02.034.

Bradford, M.M., 1976. A rapid and sensitive method for the quantitation of microgram quantities of protein utilizing the principle of protein-dye binding. Anal. Biochem. 72, 248–254. https://doi.org/10.1006/abio.1976.9999.

Brites, F., Martin, M., Guillas, I., Kontush, A., 2017. Antioxidative activity of high-density lipoprotein (HDL): mechanistic insights into potential clinical benefit. BBA Clin. 8, 66–77. https://doi.org/10.1016/j.bbacli.2017.07.002.

Bush, H., Golabi, P., Younossi, Z.M., 2017. Pediatric non-alcoholic fatty liver disease. Children 4 (6), 48. https://doi.org/10.3390/children4060048.

Cerelli, M.J., Grimm, K., Duan, X., Mulberg, E., Jalilie, M., Sekella, P., Payes, M., Cox, H., Blick, K.E., Fang, K.C., Zychlinsky, E., 2016. Evaluation of recombinant enzyme calibration to harmonize lipoprotein-associated phospholipase A2 activity results between instruments. Clin. Biochem. 49 (6), 480–485. https://doi.org/10.1016/j.clinbiochem.2015.11.018.

Cieri, R.L., 2019. Pulmonary smooth muscle in vertebrates: a comparative review of structure and function. Integr. Comp. Biol. 59 (1), 10–28. https://doi.org/10.1093/icb/icz002.

Chenxu, G., Minxuan, X., Yuting, Q., Tingting, G., Jinxiao, L., Mingxing, W., Sujun, W., Yongjie, M., Deshuai, L., Qiang, L., Linfeng, H., Jun, T., 2018. iRhom2 loss alleviates

renal injury in long-term PM2.5-exposed mice by suppression of inflammation and oxidative stress. Redox Biol. 19, 147–157. https://doi.org/10.1016/j.redox.2018.08.009.

Cliff, R., Curran, J., Hirota, J.A., Brauer, M., Feldman, H., Carlsten, C., 2016. Effect of diesel exhaust inhalation on blood markers of inflammation and neurotoxicity: a controlled, blinded crossover study. Inhal. Toxicol. 28 (3), 145–153. https://doi.org/10.3109/08958378.2016.1145770.

Cotrim, H.P., Andrade, Z.A., Parana, R., Portugal, M., Lyra, L.G., Freitas, L.A., 1999. Nonalcoholic steatohepatitis: a toxic liver disease in industrial workers. Liver 19 (4), 299–304. https://doi.org/10.1111/j.1478-3231.1999.tb00053.x.

Deng, H., Eckel, S.P., Liu, L., Lurmann, F.W., Cockburn, M.G., Gilliland, F.D., 2017. Particulate matter air pollution and liver cancer survival. Int. J. Cancer 141 (4), 744–749. https://doi.org/10.1002/ijc.30779.

Diaz-Sanchez, D., Penichet-Garcia, M., Saxon, A., 2000. Diesel exhaust particles directly induce activated mast cells to degranulate and increase histamine levels and symptom severity. J. Allergy Clin. Immunol. 106 (6), 1140–1146. https://doi.org/10.1067/mai.2000.111144.

Doeing, D.C., Solway, J., 2013. Airway smooth muscle in the pathophysiology and treatment of asthma. J. Appl. Physiol. 114 (7), 834–843. https://doi.org/10.1152/japplphysiol.00950.2012.

Dreher, K.L., Jaskot, R.H., Lehmann, J.R., Richards, J.H., McGee, J.K., Ghio, A.J., Costa, D.L., 1997. Soluble transition metals mediate residual oil fly ash induced acute lung injury. J. Toxicol. Environ. Health 50 (3), 285–305.

Emery, P.W., 2005. Metabolic changes in malnutrition. Eye 19 (10), 1029–1034. https://doi.org/10.1038/sj.eye.6701959.

Falcone, J.A., Salameh, T.S., Yi, X., Cordy, B.J., Mortell, W.G., Kabanov, A.V., Banks, W. A., 2014. Intranasal administration as a route for drug delivery to the brain: evidence for a unique pathway for albumin. J. Pharmacol. Exp. Therapeut. 351 (1), 54–60. https://doi.org/10.1124/jpet.114.216705.

Fandiño, J., Toba, L., González-Matías, L.C., Diz-Chaves, Y., Mallo, F., 2019. Perinatal undernutrition, metabolic hormones, and lung development. Nutrients 11 (12), 2870. https://doi.org/10.3390/nu11122870.

Ferraro, S.A., Yakisich, J.S., Gallo, F.T., Tasat, D.R., 2011. Simvastatin pretreatment prevents ambient particle-induced lung injury in mice. Inhal. Toxicol. 23 (14), 889–896. https://doi.org/10.3109/08958378.2011.623195.

Furlong, C.E., Richter, R.J., Seidel, S.L., Costa, L.G., Motulsky, A.G., 1989. Spectrophotometric assays for the enzymatic hydrolysis of the active metabolites of chlorpyrifos and parathion by plasma paraoxonase/arylesterase. Anal. Biochem. 180 (2), 242–247. https://doi.org/10.1016/0003-2697(89)90424-7.

Garcia, E., Stratakis, N., Valvi, D., Maitre, L., Varo, N., Aasvang, G.M., Andrusaityte, S., Basagana, X., Casas, M., de Castro, M., Fossati, S., Grazuleviciene, R., Heude, B., Hoek, G., Krog, N.H., McEachan, R., Nieuwenhuijsen, M., Roumeliotaki, T., Slama, R., Urquiza, J., et al., 2021. Prenatal and childhood exposure to air pollution and traffic and the risk of liver injury in European children. Environmental epidemiology (Philadelphia, Pa.) 5 (3), e153. https://doi.org/10.1097/EE9.0000000000000153.

Ghio, A.J., Silbajoris, R., Carson, J.L., Samet, J.M., 2002. Biologic effects of oil fly ash. Environ. Health Perspect. 110 (Suppl. 1), 89–94. https://doi.org/10.1289/ehp.02110s1189. Suppl 1.

Herriges, M., Morrisey, E.E., 2014. Lung development: orchestrating the generation and regeneration of a complex organ. Development (Cambridge, England) 141 (3), 502–513. https://doi.org/10.1242/dev.098186.

Institute for Health Metrics and Evaluation (IHME), 2024. GBD Results. IHME, University of Washington, Seattle, WA. https://vizhub.healthdata.org/gbd-results/(linki sexternal. (Accessed 4 November 2024).

Jha, V., Garcia-Garcia, G., Iseki, K., Li, Z., Naicker, S., Plattner, B., Saran, R., Wang, A.Y., Yang, C.W., 2013. Chronic kidney disease: global dimension and perspectives. Lancet (London, England) 382 (9888), 260–272. https://doi.org/10.1016/S0140-6736(13)60687-X.

Jiang, Y., Zhao, Y., Wang, Q., Chen, H., Zhou, X., 2020. Fine particulate matter exposure promotes M2 macrophage polarization through inhibiting histone deacetylase 2 in the pathogenesis of chronic obstructive pulmonary disease. Ann. Transl. Med. 8 (20), 1303. https://doi.org/10.21037/atm-20-6653.

Kim, J.W., Park, S., Lim, C.W., Lee, K., Kim, B., 2014. The role of air pollutants in initiating liver disease. Toxicol. Res. 30 (2), 65–70. https://doi.org/10.5487/TR.2014.30.2.065.

Knuckles, T.L., Jaskot, R., Richards, J.H., Miller, C.A., Ledbetter, A., McGee, J., Linak, W. P., Dreher, K.L., 2013. Biokinetically-based in vitro cardiotoxicity of residual oil fly ash: hazard identification and mechanisms of injury. Cardiovasc. Toxicol. 13 (4), 426–437. https://doi.org/10.1007/s12012-013-9225-z.

Kodavanti, U.P., Hauser, R., Christiani, D.C., Meng, Z.H., McGee, J., Ledbetter, A., Richards, J., Costa, D.L., 1998. Pulmonary responses to oil fly ash particles in the rat differ by virtue of their specific soluble metals. Toxicol. Sci. : an official journal of the Society of Toxicology 43 (2), 204–212. https://doi.org/10.1006/toxs.1998.2460.

Kodavanti, U.P., Schladweiler, M.C., Ledbetter, A.D., Hauser, R., Christiani, D.C., McGee, J., Richards, J.R., Costa, D.L., 2002. Temporal association between pulmonary and systemic effects of particulate matter in healthy and cardiovascular compromised rats. J. Toxicol. Environ. Health, Part A 65 (20), 1545–1569. https://doi.org/10.1080/00984100290071667.

Kurtz, M.L., Astort, F., Lezon, C., Ferraro, S.A., Maglione, G.A., Orona, N.S., Friedman, S. M., Boyer, P.M., Tasat, D.R., 2018. Oxidative stress response to air particle pollution in a rat nutritional growth retardation model. J. Toxicol. Environ. Health, Part A 81 (20), 1028–1040. https://doi.org/10.1080/15287394.2018.1519747.

Kurtz, M.L., Orona, N.S., Lezón, C., Defosse, V.C., Astort, F., Maglione, G.A., Boyer, P.M., Tasat, D.R., 2024a. Decreased immune response in undernourished rats after air pollution exposure. Environ. Toxicol. Pharmacol. 107, 104400. https://doi.org/10.1016/j.etap.2024.104400.

Kurtz, M., Lezón, C., Masci, I., Boyer, P., Brites, F., Bonetto, J., Bozal, C., Álvarez, L., Tasat, D., 2024b. Air pollution induces morpho-functional, biochemical and biomechanical vascular dysfunction in undernourished rats. Food Chem. Toxicol.: an international journal published for the British Industrial Biological Research Association 190, 114777. https://doi.org/10.1016/j.fct.2024.114777.

Lee, D.U., Ji, M.J., Kang, J.Y., Kyung, S.Y., Hong, J.H., 2017. Dust particles-induced intracellular Ca2+ signaling and reactive oxygen species in lung fibroblast cell line MRC5. KOREAN J. PHYSIOL. PHARMACOL.: official journal of the Korean Physiological Society and the Korean Society of Pharmacology 21 (3), 327–334. https://doi.org/10.4196/kjpp.2017.21.3.327.

Leite, F.M., Ferreira, H.daS., Bezerra, M.K., Assunção, M.L., Horta, B.L., 2013. Food intake and nutritional status of preschool from maroon communities of the state Alagoas, Brazil. Revista paulista de pediatria: orgao oficial da Sociedade de Pediatria de Sao Paulo 31 (4), 444–451. https://doi.org/10.1590/S0103-05822013000400005.

Leong, B.K., Coombs, J.K., Sabaitis, C.P., Rop, D.A., Aaron, C.S., 1998. Quantitative morphometric analysis of pulmonary deposition of aerosol particles inhaled via intratracheal nebulization, intratracheal instillation or nose-only inhalation in rats. J. Appl. Toxicol.: J. Anal. Toxicol. 18 (2), 149–160. https://doi.org/10.1002/(sici)1099-1263(199803/04)18:2<149::aid-jat490>3.0.co;2-l.

Lezón, C.E., Olivera, M.I., Bozzini, C., Mandalunis, P., Alippi, R.M., Boyer, P.M., 2009. Improved bone status by the beta-blocker propranolol in an animal model of nutritional growth retardation. Br. J. Nutr. 101 (11), 1616–1620. https://doi.org/10.1017/s000711450811145x.

Li, F., Xu, M., Wang, M., Wang, L., Wang, H., Zhang, H., Chen, Y., Gong, J., Zhang, J.J., Adcock, I.M., Chung, K.F., Zhou, X., 2018. Roles of mitochondrial ROS and NLRP3 inflammasome in multiple ozone-induced lung inflammation and emphysema. Respir. Res. 19 (1), 230. https://doi.org/10.1186/s12931-018-0931-8.

Li, M., Reynolds, C.M., Segovia, S.A., Gray, C., Vickers, M.H., 2015. Developmental programming of nonalcoholic fatty liver disease: the effect of early life nutrition on susceptibility and disease severity in later life. BioMed Res. Int. 2015, 437107. https://doi.org/10.1155/2015/437107.

Li, Y., Chi, L., Stechschulte, D.J., Dileepan, K.N., 2001. Histamine-induced production of interleukin-6 and interleukin-8 by human coronary artery endothelial cells is enhanced by endotoxin and tumor necrosis factor-alpha. Microvasc. Res. 61 (3), 253–262. https://doi.org/10.1006/mvre.2001.2304.

Li, Y., Henze, D.K., Jack, D., Henderson, B.H., Kinney, P.L., 2016. Assessing public health burden associated with exposure to ambient black carbon in the United States. Sci. Total Environ. 539, 515–525. https://doi.org/10.1016/j.scitotenv.2015.08.129.

Lifshitz, F., Moses, N., 1988. Nutritional dwarfing: growth, dieting, and fear of obesity. J. Am. Coll. Nutr. 7 (5), 367–376. https://doi.org/10.1080/07315724.1988.10720254.

Lifshitz, F., Moses, N., 1989. Growth failure. A complication of dietary treatment of hypercholesterolemia. Am. J. Dis. Child. 143 (5), 537–542, 1960.

Lifshitz, F., Pintos, P.M., Lezón, C.E., Macri, E.V., Friedman, S.M., Boyer, P.M., 2012. Dyslipidemia is not associated with cardiovascular disease risk in an animal model of mild chronic suboptimal nutrition. Nutr. Res. (N.Y.) 32 (1), 52–58. https://doi.org/10.1016/j.nutres.2011.11.002.

Liu, M., Gao, M., Hu, D., Hu, J., Wu, J., Chen, Z., Chen, J., 2024. Prolonged exposure to air pollution and risk of acute kidney injury and related mortality: a prospective cohort study based on hospitalized AKI cases and general population controls from the UK Biobank. BMC Publ. Health 24 (1), 2911. https://doi.org/10.1186/s12889-024-20321-2.

Llesuy, S., Evelson, P., González-Flecha, B., Peralta, J., Carreras, M.C., Poderoso, J.J., Boveris, A., 1994. Oxidative stress in muscle and liver of rats with septic syndrome. Free Radic. Biol. Med. 16 (4), 445–451. https://doi.org/10.1016/0891-5849(94)90121-x.

Maehly, A.C., Chance, B., 1954. The assay of catalases and peroxidases. Methods Biochem. Anal. 1, 357–424. https://doi.org/10.1002/9780470110171.ch14.

Maglione, G.A., Kurtz, M.L., Orona, N.S., Astort, F., Brites, F., Morales, C., Berra, A., Tasat, D.R., 2020. Changes in extrapulmonary organs and serum enzyme biomarkers after chronic exposure to Buenos Aires air pollution. Environ. Sci. Pollut. Res. Int. 27 (13), 14529–14542. https://doi.org/10.1007/s11356-020-07996-x.

Magnani, N.D., Marchini, T., Tasat, D.R., Alvarez, S., Evelson, P.A., 2011. Lung oxidative metabolism after exposure to ambient particles. Biochem. Biophys. Res. Commun. 412 (4), 667–672. https://doi.org/10.1016/j.bbrc.2011.08.021.

Mahrooz, A., 2024. Pleiotropic functions and clinical importance of circulating HDL-PON1 complex. Adv. Clin. Chem. 121, 132–171. https://doi.org/10.1016/bs.acc.2024.04.003.

Manzano-León, N., Serrano-Lomelin, J., Sánchez, B.N., Quintana-Belmares, R., Vega, E., Vázquez-López, I., Rojas-Bracho, L., López-Villegas, M.T., Vadillo-Ortega, F., De Vizcaya-Ruiz, A., Perez, I.R., O'Neill, M.S., Osornio-Vargas, A.R., 2016. TNFα and IL-6 responses to particulate matter in vitro: variation according to PM size, season, and polycyclic aromatic hydrocarbon and soil content. Environ. Health Perspect. 124 (4), 406–412. https://doi.org/10.1289/ehp.1409287.

Martin, M., Davico, B., Verona, M.F., Tetzlaff, W.F., Lozano Chiappe, E., Gilligan, L., Jimenez, G., Gomez Rosso, L., Ballerini, G., Boero, L., Verona, J., Brites, F., 2023. Impaired HDL-associated enzymes and proteins in children and adolescents with weight disorders and their association with novel cardiometabolic indexes. Nutr. Metabol. Cardiovasc. Dis.: Nutr. Metabol. Cardiovasc. Dis. 33 (12), 2517–2526. https://doi.org/10.1016/j.numecd.2023.08.019.

McClain, C., Vatsalya, V., Cave, M., 2017. Role of zinc in the development/progression of alcoholic liver disease. Curr. Treat. Options Gastroenterol. 15 (2), 285–295. https://doi.org/10.1007/s11938-017-0132-4.

Mills, N.L., Donaldson, K., Hadoke, P.W., Boon, N.A., MacNee, W., Cassee, F.R., Sandström, T., Blomberg, A., Newby, D.E., 2009. Adverse cardiovascular effects of air pollution. Nat. Clin. Pract. Cardiovasc. Med. 6 (1), 36–44. https://doi.org/10.1038/ncpcardio1399.

Mills, N.L., Miller, M.R., Lucking, A.J., Beveridge, J., Flint, L., Boere, A.J., Fokkens, P.H., Boon, N.A., Sandstrom, T., Blomberg, A., Duffin, R., Donaldson, K., Hadoke, P.W., Cassee, F.R., Newby, D.E., 2011. Combustion-derived nanoparticulate induces the adverse vascular effects of diesel exhaust inhalation. Eur. Heart J. 32 (21), 2660–2671. https://doi.org/10.1093/eurheartj/ehr195.

Misra, H.P., Fridovich, I., 1972. The role of superoxide anion in the autoxidation of epinephrine and a simple assay for superoxide dismutase. J. Biol. Chem. 247 (10), 3170–3175.

Orona, N.S., Astort, F., Maglione, G.A., Saldiva, P.H., Yakisich, J.S., Tasat, D.R., 2014. Direct and indirect air particle cytotoxicity in human alveolar epithelial cells. Toxicol. Vitro: an international journal published in association with BIBRA 28 (5), 796–802. https://doi.org/10.1016/j.tiv.2014.02.011.

Orona, N.S., Astort, F., Maglione, G.A., Ferraro, S.A., Martin, M., Morales, C., Mandalunis, P.M., Brites, F., Tasat, D.R., 2020. Hazardous effects of urban air particulate matter acute exposure on lung and extrapulmonary organs in mice. Ecotoxicol. Environ. Saf. 190, 110120. https://doi.org/10.1016/j.ecoenv.2019.110120.

Ostachuk, A., Evelson, P., Martin, S., Dawidowski, L., Sebastián Yakisich, J., Tasat, D.R., 2008. Age-related lung cell response to urban Buenos Aires air particle soluble fraction. Environ. Res. 107 (2), 170–177. https://doi.org/10.1016/j.envres.2008.01.007.

Paoin, K., Pharino, C., Vathesatogkit, P., Buya, S., Saranburut, K., Phosri, A., Ueda, K., Tesoro Seposo, X., Ingviya, T., Kitiyakara, T., Thongmung, N., Sritara, P., 2023. Long-term associations of air pollution exposure with liver enzymes among adult employees of the Electricity Generating Authority of Thailand: a longitudinal cohort study. Atmos. Environ. 299. https://doi.org/10.1016/j.atmosenv.2023.119648.

Parenti, M., McClorry, S., Maga, E.A., Slupsky, C.M., 2021. Metabolomic changes in severe acute malnutrition suggest hepatic oxidative stress: a secondary analysis. Nutr. Res. (N.Y.) 91, 44–56. https://doi.org/10.1016/j.nutres.2021.05.005.

Pauwels, R.A., Buist, A.S., Calverley, P.M., Jenkins, C.R., Hurd, S.S., GOLD Scientific Committee, 2001. Global strategy for the diagnosis, management, and prevention of chronic obstructive pulmonary disease. NHLBI/WHO Global Initiative for Chronic Obstructive Lung Disease (GOLD) Workshop summary. Am. J. Respir. Crit. Care Med. 163 (5), 1256–1276. https://doi.org/10.1164/ajrccm.163.5.2101039.

Pope 3rd, C.A., Burnett, R.T., Thurston, G.D., Thun, M.J., Calle, E.E., Krewski, D., Godleski, J.J., 2004. Cardiovascular mortality and long-term exposure to particulate air pollution: epidemiological evidence of general pathophysiological pathways of disease. Circulation 109 (1), 71–77. https://doi.org/10.1161/01.CIR.0000108927.80044.7F.

Pope 3rd, C.A., Burnett, R.T., Turner, M.C., Cohen, A., Krewski, D., Jerrett, M., Gapstur, S.M., Thun, M.J., 2011. Lung cancer and cardiovascular disease mortality associated with ambient air pollution and cigarette smoke: shape of the exposure-response relationships. Environ. Health Perspect. 119 (11), 1616–1621. https://doi.org/10.1289/ehp.1103639.

Pope 3rd, C.A., Bhatnagar, A., McCracken, J.P., Abplanalp, W., Conklin, D.J., O'Toole, T., 2016. Exposure to fine particulate air pollution is associated with endothelial injury and systemic inflammation. Circ. Res. 119 (11), 1204–1214. https://doi.org/10.1161/CIRCRESAHA.116.309279.

Rao, K.N., Brown, M.A., 2008. Mast cells: multifaceted immune cells with diverse roles in health and disease. Ann. N. Y. Acad. Sci. 1143, 83–104. https://doi.org/10.1196/annals.1443.023.

Rao, X., Zhong, J., Brook, R.D., Rajagopalan, S., 2018. Effect of particulate matter air pollution on cardiovascular oxidative stress pathways. Antioxidants Redox Signal. 28 (9), 797–818. https://doi.org/10.1089/ars.2017.7394.

Romieu, I., Samet, J.M., Smith, K.R., Bruce, N., 2002. Outdoor air pollution and acute respiratory infections among children in developing countries. J. Occup. Environ. Med. 44 (7), 640–649. https://doi.org/10.1097/00043764-200207000-00010.

Schneider, A., Neas, L.M., Graff, D.W., Herbst, M.C., Cascio, W.E., Schmitt, M.T., Buse, J. B., Peters, A., Devlin, R.B., 2010. Association of cardiac and vascular changes with ambient PM2.5 in diabetic individuals. Part. Fibre Toxicol. 7, 14. https://doi.org/10.1186/1743-8977-7-14.

Shubham, S., Kumar, M., Sarma, D.K., Kumawat, M., Verma, V., Samartha, R.M., Tiwari, R.R., 2022. Role of air pollution in chronic kidney disease: an update on evidence, mechanisms and mitigation strategies. Int. Arch. Occup. Environ. Health 95 (5), 897–908. https://doi.org/10.1007/s00420-021-01808-6.

Siddiqui, A.T.S., Parkash, O., Hashmi, S.A., 2021. Malnutrition and liver disease in a developing country. World J. Gastroenterol. 27 (30), 4985–4998. https://doi.org/10.3748/wjg.v27.i30.4985.

Southam, D.S., Dolovich, M., O'Byrne, P.M., Inman, M.D., 2002. Distribution of intranasal instillations in mice: effects of volume, time, body position, and anesthesia. Am. J. Physiol. Lung Cell Mol. Physiol. 282 (4), L833–L839. https://doi.org/10.1152/ajplung.00173.2001.

Sridharan, G., Shankar, A.A., 2012. Toluidine blue: a review of its chemistry and clinical utility. J. Oral Maxillofac. Pathol.: JOMFP 16 (2), 251–255. https://doi.org/10.4103/0973-029X.99081.

Stephens, N.L., 2001. Airway smooth muscle. Lung 179 (6), 333–373. https://doi.org/10.1007/s004080000073.

Stocks, J., Hislop, A., Sonnappa, S., 2013. Early lung development: lifelong effect on respiratory health and disease. Lancet Respir. Med. 1 (9), 728–742. https://doi.org/10.1016/S2213-2600(13)70118-8.

Takahashi, Y., Fukusato, T., 2014. Histopathology of nonalcoholic fatty liver disease/nonalcoholic steatohepatitis. World J. Gastroenterol. 20 (42), 15539–15548. https://doi.org/10.3748/wjg.v20.i42.15539.

Thurlbeck, W.M., Müller, N.L., 1994. Emphysema: definition, imaging, and quantification. AJR. Am. J. Roentgenol. 163 (5), 1017–1025. https://doi.org/10.2214/ajr.163.5.7976869.

Troost, J.P., D'Souza, J., Buxton, M., Kshirsagar, A.V., Engel, L.S., O'Lenick, C.R., Smoyer, W.E., Klein, J., Ju, W., Eddy, S., Helmuth, M., Mariani, L.H., Kretzler, M., Trachtman, H., 2024. Elevated exposure to air pollutants accelerates primary glomerular disease progression. Kidney international reports 9 (8), 2527–2536. https://doi.org/10.1016/j.ekir.2024.05.013.

Tsai, M., Grimbaldeston, M., Galli, S.J., 2011. Mast cells and immunoregulation/immunomodulation. Adv. Exp. Med. Biol. 716, 186–211. https://doi.org/10.1007/978-1-4419-9533-9_11.

van Zutphen, T., Ciapaite, J., Bloks, V.W., Ackereley, C., Gerding, A., Jurdzinski, A., de Moraes, R.A., Zhang, L., Wolters, J.C., Bischoff, R., Wanders, R.J., Houten, S.M., Bronte-Tinkew, D., Shatseva, T., Lewis, G.F., Groen, A.K., Reijngoud, D.J., Bakker, B. M., Jonker, J.W., Kim, P.K., et al., 2016. Malnutrition-associated liver steatosis and ATP depletion is caused by peroxisomal and mitochondrial dysfunction. J. Hepatol. 65 (6), 1198–1208. https://doi.org/10.1016/j.jhep.2016.05.046.

Wellenius, G.A., Burger, M.R., Coull, B.A., Schwartz, J., Suh, H.H., Koutrakis, P., Schlaug, G., Gold, D.R., Mittleman, M.A., 2012. Ambient air pollution and the risk of acute ischemic stroke. Arch. Intern. Med. 172 (3), 229–234. https://doi.org/10.1001/archinternmed.2011.732.

Xiao, Y., Hu, J., Chen, R., Xu, Y., Pan, B., Gao, Y., Deng, Y., Li, W., Kan, H., Chen, S., 2024. Impact of fine particulate matter on liver injury: evidence from human, mice and cells. J. Hazard Mater. 469, 133958. https://doi.org/10.1016/j.jhazmat.2024.133958.

Xu, F., Shi, X., Qiu, X., Jiang, X., Fang, Y., Wang, J., Hu, D., Zhu, T., 2020. Investigation of the chemical components of ambient fine particulate matter ($PM_{2.5}$) associated with in vitro cellular responses to oxidative stress and inflammation. Environ. Int. 136, 105475. https://doi.org/10.1016/j.envint.2020.105475.

Xu, M.X., Ge, C.X., Qin, Y.T., Gu, T.T., Lou, D.S., Li, Q., Hu, L.F., Feng, J., Huang, P., Tan, J., 2019. Prolonged PM2.5 exposure elevates risk of oxidative stress-driven nonalcoholic fatty liver disease by triggering increase of dyslipidemia. Free Radic. Biol. Med. 130, 542–556. https://doi.org/10.1016/j.freeradbiomed.2018.11.016.

Xu, X., Nie, S., Ding, H., Hou, F.F., 2018. Environmental pollution and kidney diseases. Nat. Rev. Nephrol. 14 (5), 313–324. https://doi.org/10.1038/nrneph.2018.11.

Yagi, K., 1976. A simple fluorometric assay for lipoperoxide in blood plasma. Biochem. Med. 15 (2), 212–216. https://doi.org/10.1016/0006-2944(76)90049-1.

Yang, Y.S., Cao, M.D., Wang, A., Liu, Q.M., Zhu, D.X., Zou, Y., Ma, L.L., Luo, M., Shao, Y., Xu, D.D., Wei, J.F., Sun, J.L., 2022. Nano-silica particles synergistically IgE-mediated mast cell activation exacerbating allergic inflammation in mice. Front. Immunol. 13, 911300. https://doi.org/10.3389/fimmu.2022.911300.

Zhang, Y., Shi, J., Ma, Y., Yu, N., Zheng, P., Chen, Z., Wang, T., Jia, G., 2023. Association between air pollution and lipid profiles. Toxics 11 (11), 894. https://doi.org/10.3390/toxics11110894.

Zheng, J., Yue, L., Wang, B., Li, Y., Zhang, L., Xue, B., Tian, X., Lei, R., Luo, B., 2023. Seasonal characteristics of ambient temperature variation (DTR, TCN, and $TV_{0\text{-}t}$) and air pollutants on childhood asthma attack in a dry and cold city in China. Environ. Res. 217, 114872. https://doi.org/10.1016/j.envres.2022.114872.

Zhou, Y., Zou, Y., Li, X., Chen, S., Zhao, Z., He, F., Zou, W., Luo, Q., Li, W., Pan, Y., Deng, X., Wang, X., Qiu, R., Liu, S., Zheng, J., Zhong, N., Ran, P., 2014. Lung function and incidence of chronic obstructive pulmonary disease after improved cooking fuels and kitchen ventilation: a 9-year prospective cohort study. PLoS Med. 11 (3), e1001621. https://doi.org/10.1371/journal.pmed.1001621.